Chemical Geology 580 (2021) 120382

Contents lists available at ScienceDirect

Chemical Geology

journal homepage: www.elsevier.com/locate/chemgeo

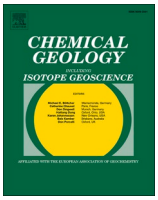

The in vacuo release of Ar from minerals: 2. The role of structural modifications of K-feldspar during heating revealed by Raman microprobe analyses

Jennifer Kung [a], Igor M. Villa [b,c,*]

[a] Department of Earth Sciences, National Cheng Kung University, Tainan, Taiwan
[b] Institut für Geologie, Universität Bern, Bern, Switzerland
[c] Centro Universitario Datazioni e Archeometria, Università di Milano Bicocca, Milano, Italy

ARTICLE INFO

Editor: Balz Kamber

ABSTRACT

The release of Ar during stepwise heating ^{39}Ar—^{40}Ar dating experiments may be controlled by Fick's Law diffusion in an inert matrix, and/or by structural modifications of the host mineral. A ca. 1 mm^3 irradiated cleavage fragment of a low sanidine crystal from Itrongay, Madagascar was degassed isothermally at 888 ± 2 °C for 264 h, acquiring 67 stepwise ^{39}Ar release data. The ^{39}Ar release was observed to follow a smooth sigmoid curve and not a line as would be predicted by Fick's Law. If the ^{39}Ar release is controlled by crystallographic changes, the implication is that these changes undergo time-dependent variations. The long-term bulk degassing, being the sum of various structural modifications, approximates a Fickian behavior that is not verified in detail in short-term experiments, as it averages over different ^{39}Ar release regimes. This would make the downslope extrapolation of laboratory data to geological conditions highly underconstrained.

In order to constrain the behavior of the crystal structure of K-feldspar during laboratory heating, we measured the Raman spectra of a different, ca. 1 mm^3 cleavage fragment of the same irradiated sanidine crystal. The sample was heated in air in a Linkam heating stage, and Raman spectra were acquired at temperatures increasing from 300 to 1000 °C, including a 6-h isothermal run at 900 ± 1 °C.

Raman modes between 50 and 1200 cm^{-1} were observed to record two kinds of change, defining robust trends. The positions of most peaks were shifted towards lower wavenumbers (lower energies) and broadened; in addition, the relative heights of different peaks showed robust variation trends. The larger changes coincide with discrete temperature increases, but all changes also progressed over time at constant temperature. These peaks mirror the excitation of phonon modes, which are associated with interatomic bond stretching and deformation, with Si,Al ordering and with deformation and rotation of SiO_2 tetrahedra. Most, but by far not all, of the change is reversible (such as e.g. the differential activation of phonon modes), but irreversible structure modifications (such as e.g. Al,Si disordering) are also recorded. We conclude that the K-feldspar structure violates mathematical requirements of matrix inertness during laboratory heating.

1. Introduction

Hydrous minerals frequently used in ^{39}Ar—^{40}Ar dating (amphiboles, micas) release their Ar during in vacuo heating when their crystal structure is distorted by dehydration (Villa, 2021). Another mineral widely used in ^{39}Ar—^{40}Ar dating is K-feldspar (Kfs), whose Ar retention has attracted considerable interest in the literature (see e.g. the review by Chafe et al., 2014). Feldspars are nominally anhydrous and thus not destabilized by dehydration. However, in practically all terrestrial rocks that have been studied in sufficient detail, feldspars are observed to record retrograde reactions. The fundamental importance of petrologic groundwork, a routine prerequisite for U—Pb dating for the last 30 years, was underappreciated in several ^{39}Ar—^{40}Ar dating studies. Petrographic investigations by EPMA (electron probe microanalyzer), CL (cathodoluminescence) and TEM (transmission electron microscope) demonstrate that even feldspars viewed as "diffusion archetypes" consist of half a dozen different phases produced by chemically open-system reactions (Chafe et al., 2014), most of whom have demonstrably

* Corresponding author at: Institut für Geologie, Universität Bern, Bern, Switzerland.
E-mail address: igor@geo.unibe.ch (I.M. Villa).

https://doi.org/10.1016/j.chemgeo.2021.120382
Received 30 January 2021; Received in revised form 2 June 2021; Accepted 6 June 2021
Available online 8 June 2021

higher Ar transport rates than Kfs sensu stricto. Lunar and most meteoritic feldspars were spared interaction with aqueous fluids, yet sample availability limits the effectivity of mineral separation, so much so that the analyzed samples are never monomineralic (e.g. Turner et al., 1971). It follows that the stepheating $^{39}Ar—^{40}Ar$ analyses of extraterrestrial samples cannot provide accurate extrapolations of their thermal history, as the Ar degassing rate of a polymineralic mixture is not a function of a single variable.

In exceptional cases of truly monomineralic, unretrogressed Kfs it had been observed (Foland, 1994, his Figs. 15–16; Villa, 1996, his Fig. 1) that the ^{39}Ar release did not follow linear trajectories in Arrhenius diagrams as heating schedules were modified, especially when the heating schedule included isothermal heating steps. This runs counter the models that assume Fick's Law diffusion as the exclusive control on Ar transport; however, it was not entirely suprising from first principles of quantum mechanics (Panzarini and Colombo, 1994a, 1994b). These authors used molecular dynamics to calculate the diffusion of one hydrogen atom in a supercell of 64 Si atoms; they found a large number of violations of Fick's Law. They were first in attributing a decisive role of phonons in non-linear modulations of hydrogen transport. Phonons are collective vibration modes of atoms, a typical quantum mechanical phenomenon that was unknown in continuum physics during the 19th century. Both Fourier Fourier's (1822) treatment of heat diffusion and its adaptation to nutrient transport in aqueous solutions by Fick (1855) explicitly assume an inert matrix and continuum mechanics. Panzarini and Colombo (1994b, p. 146) explicitly stated that "extrapolation of the Arrhenius plot down to room temperature turns out to be questionable". They calculated that upon heating the Si crystalline matrix undergoes discrete structural modifications, which cause discrete jumps in pre-exponential factors and activation energies. Any macroscopic mathematical description of diffusion can account for variable boundary conditions but not for time-dependent matrix variations (cfr. Crank, 1975).

The transport of Ar is practically certain to show even larger deviations from models based on Fick's Law, and to be more heavily affected by structural changes of the solid matrix, than is hydrogen diffusion in silicon. The H atom is small and its movement in a crystal is least impeded of all diffusing atoms. On the contrary, the Ar atom is tightly trapped owing to its radius (1.88 Å) being much larger than that of all structure-forming ions ($\leq$ 1.4 Å) in the feldspar structure (Nyfeler et al., 1998; Du et al., 2008). This means that any movement of the Ar atom requires the creation of a vacancy. The energy budget of Ar degassing, ca. 250 kJ/mol, means that the required point defect is a Schottky defect (one cation plus one anion). It has been conjectured (Nyfeler et al., 1998) that the Al,Si disordering rate and the Ar degassing rate are similar or equal, as disordering involves the simultaneous jump of one Al and one Si ion from their current crystallographic site. This transient local lattice distortion greatly facilitates the jump of the Ar atom by one unit cell. The question is not if, but how these jumps are affected by distortions of the host mineral structure during heating. In particular, the observations by Foland (1994), confirmed by Villa (1996), demonstrate that the release rate of Ar decreases while the sample is held at constant temperature. This is evidence that structural changes are not only temperature-dependent but also time-dependent.

It has long been established (Wenk, 1978; Angel et al., 2013, and references therein) that plagioclase undergoes both displacive and irreversible structural transformations upon heating. Salje (1986) demonstrated by Raman microprobe that the albite structure is neither inert nor continuously variable, as the relative intensity of the phonon modes is not continuous but undergoes quantum transitions. His observations on albite validate the molecular dynamics calculations on metallic Si (see above) that the instantaneous crystal structure during heating is modified in discrete jumps. The implication for Ar transport in feldspars is that, since the diffusion matrix is not inert, downslope extrapolation of high-*T* degassing rates of minerals in the laboratory is not representative of Ar loss at low *T* in natural environments, as the high-*T* structure is not identical to the low-*T* structure.

A suitable sample to address the mechanism of Ar release from feldspars experimentally is the gem-quality, Fe-rich low sanidine ($K_{0.97}Na_{0.05}[Al_{0.94}Fe^{3+}_{0.05}Si_3O_8]$) from Itrongay, Madagascar. For this strictly monomineralic specimen, a bell-shaped spatial Ar gradient appears consistent with direct observations (Flude et al., 2014). However, Ar release in short-term and long-term isothermal degassing experiments was observed to not fully respect the diffusion equations (Villa, 1996; Wartho et al., 1999), in agreement with a priori arguments that require deviations from predictions of classical continuum physics (see above). The changes to the feldspar structure predicted by quantum mechanics can be either displacive (Laves, 1956) or quenchable, i.e. irreversible. Nyfeler et al. (1998) quantified the rate of irreversible Si,Al disordering during heating by quenching the crystal and performing structure refinements at room temperature. A further, apparently trivial confirmation of the modification of the extrinsic defect structure (sensu Lasaga, 1981) is coloring. The studied Itrongay crystal was honey-colored when purchased, became brownish after irradiation, and became colorless when extracted from the heating stage after the experiment. Si,Al disordering and annealing of color centers are both quenchable and were directly observed after heating. The former requires a transient formation of a Schottky point defect, which is needed for the Si,Al exchange, and which is likely exploited for the transport of the otherwise locked Ar atom (Nyfeler et al., 1998, their Fig. 1b). Color centers are best understood in terms of the band structure in solid state physics (Gordon, 1959) and may, but need not, be related to Frenkel point defects. Their annealing is exploited by thermoluminescence dating and by gemstone "enhancement" and entails a local modification of the crystal structure near a point defect.

Reversible structural modifications such as the intensity variations of phonon modes cannot be observed at room temperature (e.g. Laves, 1956) and require in-situ observations at high *T*. In order to monitor the evolution of the reversible structural modifications, both temperature-dependent and time-dependent at constant, high *T* (such as those revealed by the intensity variations of phonon modes: Zeiger et al., 1992) we decided to perform high-temperature Raman spectroscopy on the monomineralic, museum-grade Itrongay sanidine.

One unsolved question regards the time-scales of structural modifications: the isothermal diffusion experiments by Wartho et al. (1999) lasted several days, and the diffusion profiles revealed by laser microprobe depth profiling by Flude et al. (2014) were acquired over geological times. In both situations, long-term achievement of steady state may cancel out any transient behavior during the relatively short (typically 10–30 min) degassing steps of $^{39}Ar—^{40}Ar$ analyses.

A further point to be considered is the influence of neutron irradiation on the defect structure of Kfs. (Villa, 1996, his Fig. 1) suggested that the Arrhenius regression of the Ar degassing rate in an irradiated cleavage fragment of the Itrongay sanidine may have a lower activation energy than that of an unirradiated aliquot. As dating experiments are performed on irradiated samples, it is of secondary importance for the present investigation on in vacuo degassing to precisely ascertain in what respects the irradiation creates additional extrinsic point defects (e.g. Lasaga, 1981) relative to those present in unirradiated samples. The argument that in nature Kfs geochronometers lose Ar from a crystal structure with a comparatively smaller density of extrinsic point defects, whereas laboratory experiments interrogate a more defect-rich crystal structure, would only become relevant if and when there will exist studies performed on monomineralic terrestrial samples demonstrated by EPMA, CL and TEM to be devoid of any retrogression reactions.

The present work endeavors to bring into a context the process studied by geochronologists, viz. the temperature-dependent degassing of radiogenic ^{40}Ar daughter isotopes both in nature and in the laboratory, with the temperature-dependent crystallographic observations. For this purpose we performed a twin experiment at the high *T* typical of laboratory $^{39}Ar—^{40}Ar$ dating of Kfs. In one experiment we performed a very long duration isothermal Ar stepwise degassing experiment to map

out any possible deviation of the progressive Ar release from the diffusion equations. In the companion experiment, aimed at quantifying the distortion of the Kfs structure, we acquired Raman spectra at T between 300 and 1000 °C.

2. Analytical procedure

In this study, both the Ar degassing experiment and the high T Raman measurements were carried out on two ca. 1 mm^3 irradiated cleavage fragments of the same sanidine megacryst from Itrongay used by Villa (1996) and Wartho et al. (1999). A parallelepipedal fragment with a mass of 1.1 mg (approx. 1 × 1 × 0.4 mm) was degassed in 67 isothermal steps at 888 ± 2 °C for a total time of 951 ks (approx. 264 h), followed by 9 isothermal steps at 1024 ± 4 °C, and final degassing in four steps <3 ks at increasing T up to 1500 °C. A detailed description of the isothermal heating protocol and the complete ^{39}Ar release data are presented in the Supplementary Material and Supplementary Table S1.

Another 1 mm^3 fragment of the same megacryst was analyzed by Raman microprobe analysis in the Mineral Physics Laboratory of National Cheng Kung University, Tainan. Unpolarized Raman measurements were performed using a backscattering geometry (180°) with a micro-Raman system containing a 550 mm focal length spectrometer (Jobin-Yvon/Horiba). Raman spectra were excited with radiation of 458 nm (Coherent Genesis semiconductor laser). The unoriented single-crystal feldspar was loaded into the heating stage (Linkam, TS1500), whose T was raised from room temperature (RT) to 300 °C in approx. 1 min, and from there to 800 °C in 100 °C steps. T was then dropped to RT. After 12 h at RT, T was again raised to 800 °C, held for 2.5 h, and then held for 6 h at 900 ± 1 °C. Finally, T was raised to 1000 °C for 60 min. Raman spectra were acquired mostly every 30 min, starting at RT before heating and ending at RT after heating. Because a relatively large crystal area (ca. 1 × 1 mm^2) covered the heating stage, the IR radiation from the heating stage entering the return optic path was reduced, and the background of Raman spectra presented minor systematic increases as a function of T. Before the data analysis, a linear background profile was applied. Data were imported into Peakfit software, before the data analysis, a linear background profile was applied first. Then the peak positions, FWHM (full width at half maximum), and their integrated area were determined using the peak fitting utility. The uncertainty in peak position was <0.6 cm^{-1} for sharp peaks and up to ca. 10 cm^{-1} or more for the weak broad peaks.

In the following figures we plot the spectra obtained for each temperature step right after reaching thermal equilibrium. The final RT spectrum, acquired at 25 °C after cooling, is displayed arbitrarily as having been acquired at 100 °C in order to visually disambiguate the quenchable structure modification achieved after the heating.

3. Results

The complete ^{39}Ar release data are presented in Supplementary Table S1. Fig. 1 shows the observed time-dependence of the ^{39}Ar release, displayed as manifestations of the diffusion equations (Fechtig et al., 1961). The ^{39}Ar release rate is compared with the predicted Fick's Law diffusive Ar loss calculated using Crank's (1975) eq. 5.21 and the diffusivity D(888 °C) interpolated from the data by Wartho et al. (1999).

Fig. 2 shows the Raman spectrum measured at RT before the heating cycle, together with the calculated deconvolution into individual phonon modes. Fig. 3 shows a superposition of the eight high T spectra, Fig. 4 plots the shift of the peak positions with increasing T. Additional details are presented in Supplementary Figs. S1–S9.

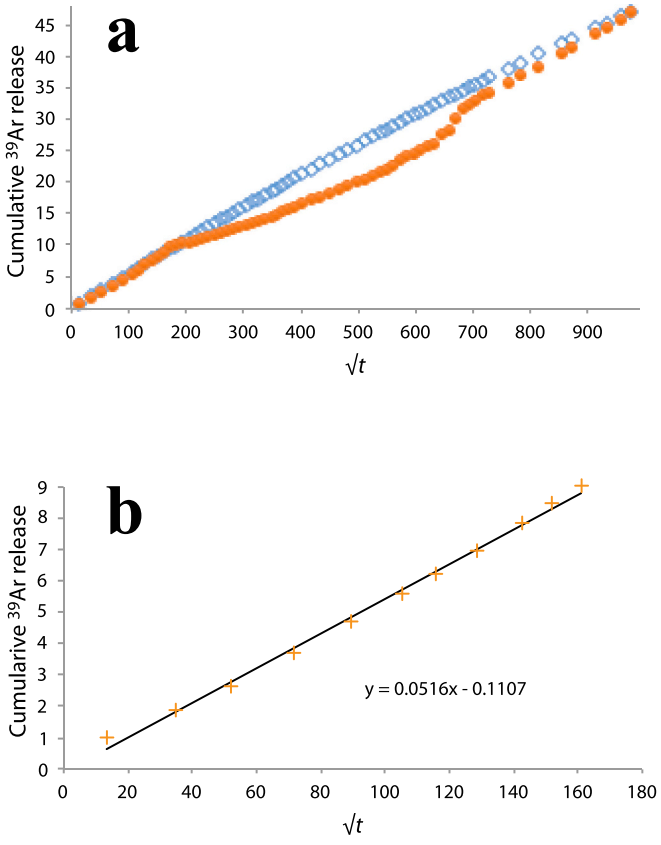

Fig. 1. ^{39}Ar degassing rates of the Itrongay sanidine during isothermal heating at 888 °C. (a) Observed degassing (filled squares) and calculated degassing (open circles) using the apparent diffusion constant determined by Wartho et al. (1999). The cumulative degassing is expressed as percentage of the total ^{39}Ar content. (b) Detail of the first 7.2 h of the isothermal heating, with a linear regression through the 11 data points.

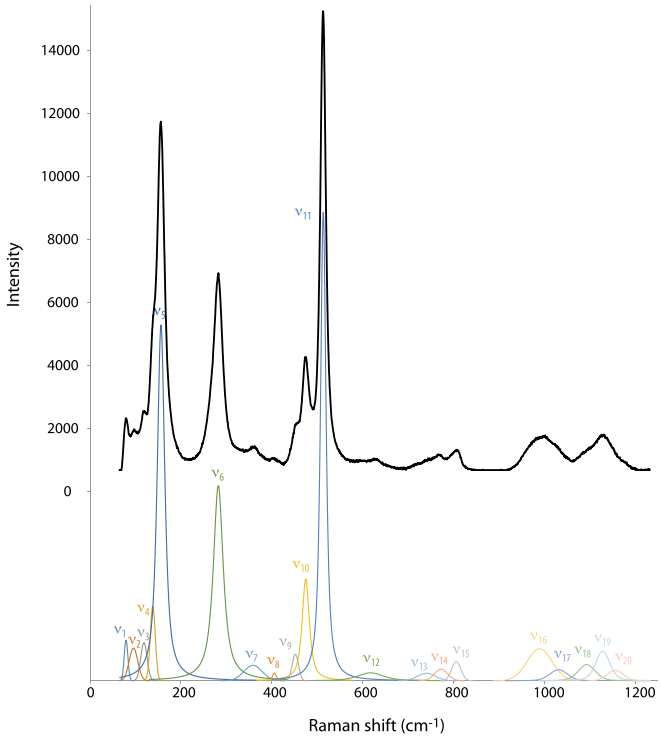

Fig. 2. Raman spectrum (black curve) of the low sanidine from Itrongay, Madagascar, collected at room temperature (RT) before heating. The deconvoluted peaks of the RT spectrum, labelled ν_1-ν_{20} as detailed in Table 1, are shown vertically offset.

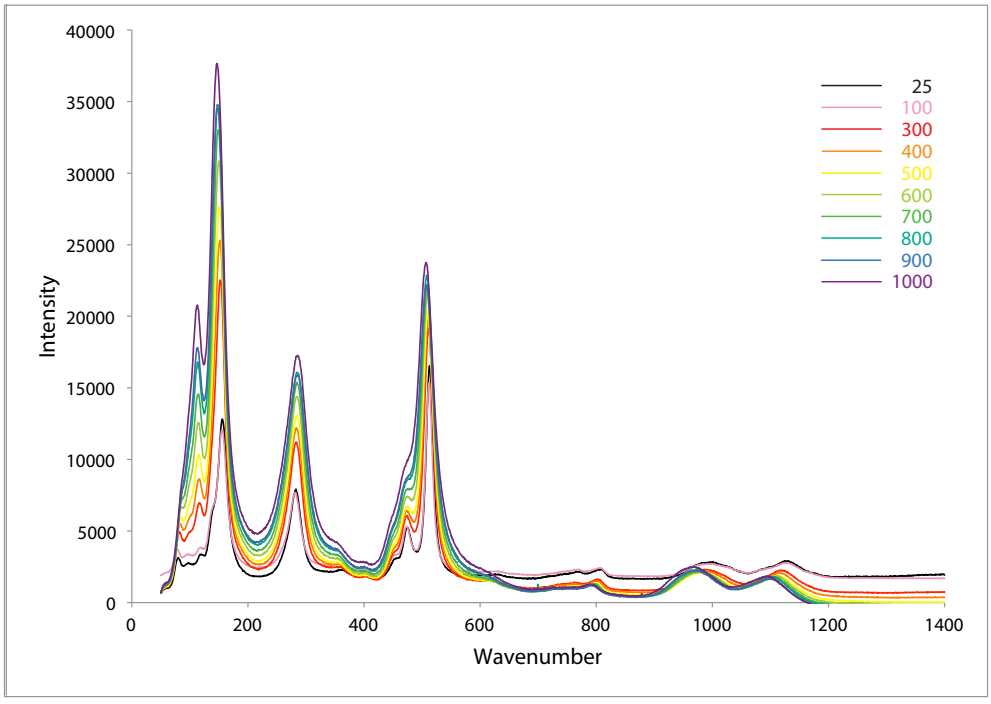

Fig. 3. Raman spectra obtained at increasing *T*. The intensity changes dramatically, especially the peaks below 600 cm^{-1}.

In the present study we identified 20 Raman modes at RT for the Itrongay sanidine, shown in Fig. 2 and tabulated in Table 1. Compared with a previous study (Freeman et al., 2008), the Raman patterns were highly similar between 150 and 1200 cm^{-1}; the peak positions were identical for most of them within ca. 5 cm^{-1} (Table 1). The differences of the peak positions for ν_5, ν_7, ν_{12}, ν_{13} and ν_{13} were larger than 10 cm^{-1}. The peak at 571 cm^{-1} observed by Freeman et al. (2008) was not observed in our sample. The Raman modes of feldspars can be interpreted in terms of crystal structure based on the classification by McKeown (2005), Freeman et al. (2008), Caracas and Bobocioiu (2011, computed spectrum "oligoclase w000121") and Aliatis et al. (2015). Following the terminology by McKeown (2005), the Raman modes are

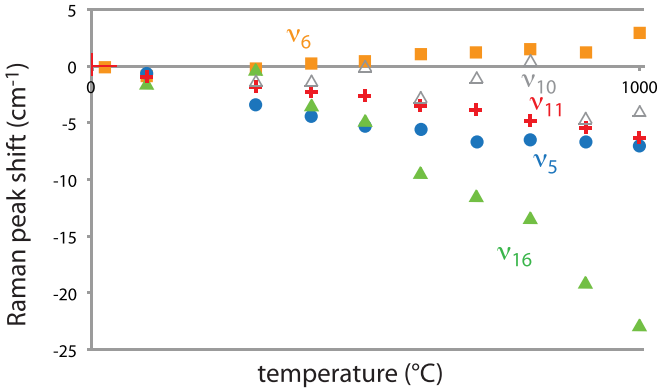

Fig. 4. Temperature-dependent shift of Raman peak positions. The shift is calculated relative to the RT measurement before the heating. The uncertainty of all position measurements is 0.6 cm^{-1}. The point plotted at the temperature labelled "100 °C" is the RT measurement at 25 °C after the heating, slightly displaced to visually display the difference between the peak positions at RT before and after the heating (see Fig. S2).

Table 1
Raman modes, wavenumber and FWHM widths of the fitted deconvolutions at room temperature.

Raman mode label	Wavenumber (cm^{-1})	Width (cm^{-1})
ν_1	79.2	9.5
ν_2	95.6	22.2
ν_3	118.6	16.6
ν_4	138.0	13.0
ν_5	156.1	19.8
ν_6	282.1	16.1
ν_7	358.4	47.4
ν_8	405.4	10.4
ν_9	451.5	16.5
ν_{10}	474.5	19.0
ν_{11}	513.0	14.5
ν_{12}	617.1	68.1
ν_{13}	740.0	46.8
ν_{14}	772.0	34.4
ν_{15}	805.5	24.0
ν_{16}	988.6	64.6
ν_{17}	1030.6	45.8
ν_{18}	1092.5	44.5
ν_{19}	1127.6	36.7
ν_{20}	1155.4	42.2

broadly grouped into three regions: lines with lowest energies (50–300 cm^{-1}, ν_1- ν_6) correspond to stretching of K—O (and Na—O) bonds, called "cage shearing"; the middle-energy region (350–800 cm^{-1}, ν_7- ν_{15}) corresponds to Si-O-Si bond bending, called "ring breathing"; the high-energy region above 900 cm^{-1} (ν_{16}- ν_{20}) is attributed to Si—O bond stretching (or "tetrahedral breathing"). Al,Si disordering (as quantified by Nyfeler et al., 1998) results in a broadening of lines (Zhang et al., 1996; McKeown, 2005; Freeman et al., 2008).

Supplementary Table S2 shows the intensity and FWHM of Raman peaks increasing with *T*. During heating, the weak peaks at the positions ν_7, ν_8 and ν_{12} and a shoulder peak, ν_4, became too difficult to deconvolute as they merged into either background or the major peak ν_5. Due to the increasing intensity, the feature of the minor Raman peaks below the 200 cm^{-1} wavenumber, ν_i ($i = 1$–3) was dominated by the growth of ν_3. The analysis of peak evolution at high *T* showed that the peaks ν_1 and ν_3 were shifting towards higher wavenumbers, in contrast to most other Raman peaks shifting to lower wavenumbers (Fig. 4).

4. Discussion

A combined mineralogical-geochronological investigation on K-feldspar can be discussed in three tiers: (1) establishment of the context between observation of crystal structure changes via Raman spectroscopy of the Itrongay sanidine and Ar release; (2) in-depth analysis of the significance of the temperature-dependent behavior of individual Raman modes and interpretation of their relevance to the details of the crystal structure (Caracas and Bobocioiu, 2011); (3) extension of the observations on the Itrongay sanidine to other K-feldspar samples of a different composition. Our study will mainly address the first tier. Once the context between crystal structure and Ar release mechanism is established, the details in the second tier will require further effort by crystallographers. It will be possible to address the third tier only when the gap between observations and modelling will be bridged, i.e. when it will be universally realized that a crystallographer's feldspar and a tectonics user's feldspars are not per se comparable minerals. K-feldspars normally used for tectonic modelling are often turbid and usually consist of μm-scale polyphase mosaics of retrograde clays, secondary veins, CL-bright patches, Ca-rich extraneous phases, and also true K-feldspar (e.g. Chafe et al., 2014).

The time-dependence of ^{39}Ar release at high *T* is displayed in Fig. 1. The results of the 67 steps at 888 °C (filled squares) are shown in Fig. 1a together with the theoretical release calculated from the diffusivity determined by Wartho et al. (1999) (open circles). Since both samples were cleavage fragments of the same 10 cm megacryst, it is assumed that their diffusivity should be identical. A broad agreement at the beginning and at the end of the isothermal run between the observed ^{39}Ar release and the theoretical calculation is apparent. However, for abscissa values between 170 and 700 $s^{1/2}$ (i.e. times between 29 and 490 ks), the trajectory of the observed Ar release follows a sigmoidal curve, whereby the cumulative ^{39}Ar release is lower than the calculation. This sigmoidal curve, however, must not be viewed as a minor, statistically random perturbation of an otherwise accurate physical description of the processes controlling Ar release from Kfs. On the contrary, the systematic nonlinear trend, associated with practically undetectable noise, is proof that classical physics of an inert crystal structure fails to accurately predict the time dependence of the Ar release.

The duration of the isothermal degassing experiment was chosen so as to provide a glimpse into the uncharted Kfs behavior under heating for durations longer than an hour (most ^{39}Ar—^{40}Ar experiments are comprised of heating steps lasting for 10–30 min) and shorter than several days (the Ar degassing data presented by Wartho et al., 1999, required heating times up to 14 d). Fig. 1b shows the uninterrupted, isothermal sequence of the first 11 heating steps and their linear regression. The use of a first-order linear regression is justified, relative to a second-order term $O(x^2)$, as the deviation from linearity for fractional Ar losses <10% (as observed here) is smaller than the graphic symbol. The upwards concave trajectory of the data points between $\sqrt{t} = 200$–700 is striking. The Ar release rate increases with $\sqrt{t}$, i.e. is controlled by the structural modifications revealed by the Raman observations (see below). The intercept of the regression line is negative (Fig. 1b), an unphysical result. A negative intercept of a quantity that must always be >0 can only be explained by regressing together two (or more) unrelated processes. In the present case, the most likely explanation is a change of the mechanism of ^{39}Ar release, which is likely to be controlled by crystallographic changes, during the 7 h period. This observation reiterates that modelling ^{39}Ar release as exclusively due Fick's Law diffusion is self-contradicting.

In a first attempt at an interpretation of the Raman data we will focus on the major modes (i.e., those with the highest amplitude, Fig. 2): cage shearing modes 118 (ν3), 156 (ν_5) and 282 (ν_6) cm^{-1}; ring breathing modes 474 (ν_{10}) and 513 (ν_{11}) cm^{-1}, which may be the most relevant to the release of Ar, as they affect the path of least resistance for the transport of the oversized Ar atom (Nyfeler et al., 1998, their Fig. 1b); and tetrahedral breathing mode 988 (ν_{16}) cm^{-1}. A note of caution is that

our data set consists of only nine temperature steps (RT plus heating steps from 300 to 1000 °C); the possibility to resolve fine effects is limited. One such effect that would require further dedicated investigation is the break in slope in the temperature-dependent trends between 800 and 900 °C visible in Supplementary Figs. S7–S8.

The similarity of the Raman spectra obtained at RT before and after the heating cycles (Fig. 2 and Supplementary Fig. S2) demonstrate that most structural changes are reversible. The irreversible change shown by the slightly but resolvably shifted peaks (Supplementary Fig. S2) is much smaller than the peak shifts at high *T* (Fig. 3 and Supplementary Figs. S3–S6). This justifies a posteriori the decision to acquire Raman spectra at high-*T* in order to fully appreciate the vastly predominant reversible transformations.

Under applied field (e.g., *P* and *T*), the Raman peak position moves to higher wavenumber at increasing *P*, interpreted as bond shortening, and to lower wavenumber at increasing *T*, interpreted as bond lengthening (e.g., Richet et al., 1998; Yang et al., 1999). In our experiment, the Raman peaks are significantly changed with increasing *T* in terms of position, width, absolute intensity, and relative intensity. Upon heating, most peak locations are shifted towards the left, i.e. lower energy (Fig. 3 and Supplementary Figs. S3–S6; cf. Liu et al., 2018). Among the higher intensity peaks, the 282 cm^{-1} peak (ν_6) defines an antithetic trend (Supplementary Fig. S4), shifting towards higher wavenumbers at higher *T* (other minor peaks also follow this antithetic trend: see Supplementary Table S2). Antithetic shifts are not an exceptional observation, and had been calculated for zircon by Stangarone et al. (2019, their Fig. 5). Both absolute peak intensities and widths (Fig. 2 and Supplementary Fig. S7) increased with increasing *T*. The intensity increase is observed on all the major peaks. This runs counter previous investigations on ordered and disordered feldspars (e.g. Salje, 1986), who observed decreasing intensities with increasing *T*. A detailed crystallographic explanation of our ubiquitous observation of amplitude increase at increasing *T* exceeds the purpose of the present paper, which is devoted to establishing the link between temperature-dependent structural modifications and the release of Ar in vacuo. Whatever the cause of the intensity variation, the ratio of the peak intensities is likely to cancel it out and to reflect the relative importance of the respective phonon modes. In the present experiment, the ratios of the intensities of the six major peaks also change substantially with increasing *T* (Supplementary Fig. S8). This reflects a large variation of the importance of the major phonon modes. The increased thermal energy in the different temperature steps does not cause a uniform increase of all vibration modes: instead, it is partitioned heterogeneously among the modes. When the vibrations that modify the ring opening (modes at 474 and 513 cm^{-1}) are enhanced or reduced, the degassing of Ar from the crystal is disproportionately increased or decreased.

We observed that the Raman spectra of the Madagascar sanidine recorded only barely resolvable shifts during the 350 min spent at 900 °C (Supplementary Fig. S9). This is consistent with the observations by Nyfeler et al. (1998), who were able to resolve Si,Al disordering (within the limits of structural refinement) only for a 950 °C heating duration of 672 h, but not for one of 12 h.

We interpret the Raman observations as strong evidence that the Madagascar sanidine underwent three kinds of discrete crystallographic changes with increasing *T*: (i) changes in K—O bond lengths, (ii) bending of Si-O-Si bonds, and (iii) tetrahedral breathing. The non-linear time dependence of the ^{39}Ar degassing rate (especially the negative intercept, see above) require a change of degassing mechanism. A reasonable implication is that the bond length variations modify the formation rate of the Schottky defects necessary for the migration of Ar atoms. The growing importance of the ν_{16} mode with increasing *T* supports the conjecture by Hetherington and Villa (2007) that Ar degassing of silicates is enhanced by deformation of the tetrahedral framework.

5. Conclusions

The Kfs matrix not only deviates from inertness due to discrete excitation of phonon modes that pertain to stretching of K—O bonds, deformation of the ring, and rotation of the Si tetrahedra. It also undergoes progressive, irreversible disordering. The short-term (7 h) Ar degassing of sanidine is influenced by crystallographic changes. To first order, the Ar release rate is coarsely compatible with Fick's Law; however, both our crystallographic interpretation of the Raman microprobe observations and the ^{39}Ar degassing trends in the long-time isothermal heating experiment unambiguously demonstrate that this is not accurate. One important effect is certainly Si,Al disordering, which is an irreversible modification of the matrix. Reversible structural modifications, such as the differential excitation of phonon modes, are also documented here; charting their effect on the Ar release of other K-feldspar samples would need additional investigations. However, the unsurmountable difficulty for such desirable experiments is finding truly monomineralic feldspars that are devoid of retrogression phases.

Supplementary data to this article can be found online at https://doi.org/10.1016/j.chemgeo.2021.120382.

Declaration of Competing Interest

The authors declare that they have no known competing financial interests or personal relationships that could have appeared to influence the work reported in this paper.

Acknowledgements

The installation of Raman spectroscope in Tainan was funded by the Ministry of Science and Technology, grant numbers MOST 105-216-M-006-019 to J.K., and partially supported by the grants from the "Core Facility Center", National Cheng Kung University, and "Geochemical Precious Instrument Platform Project: Southern Branch Ministry of Science". The Noblesse mass spectrometer in Milan was funded and is maintained by Università di Milano Bicocca, grant 2016-ECOT-0044 to I.M.V. Laboratory maintainance by V. Barberini, S.-C. Chung and F.T.S. Hua is gratefully acknowledged. This manuscript benefited from comments by A.R. Heri and M.L. Frezzotti. Reviews by two anonymous referees and by Editor Balz Kamber greatly helped in focusing our presentation.

References

Aliatis, I., Lambruschi, E., Mantovani, L., Bersani, D., Andò, S., Gatta, G.D., Gentile, P., Salvioli-Mariani, E., Prencipe, M., Tribaudino, M., Lottici, P.P., 2015. A comparison between *ab initio* calculated and measured Raman spectrum of triclinic albite ($NaAlSi_3O_8$). J. Raman Spectrosc. 46, 501–508.

Angel, R.J., Ross, N.L., Zhao, J., Sochalski-Kolbus, L., Krüger, H., Schmidt, B.C., 2013. Structural controls on the anisotropy of tetrahedral frameworks: the example of monoclinic feldspars. Eur. J. Mineral. 25, 597–614.

Caracas, R., Bobocioiu, E., 2011. The WURM project—a freely available web-based repository of computed physical data for minerals. Am. Mineral. 96, 437–443.

Chafe, A.N., Villa, I.M., Hanchar, J.M., Wirth, R., 2014. A re-examination of petrogenesis and ^{40}Ar/^{39}Ar systematics in the the Chain of Ponds K-feldspar: "diffusion domain" archetype versus polyphase hygrochronology. Contrib. Mineral. Petrol. 167 (5), 1010.

Crank, J., 1975. The Mathematics of Diffusion, Second edition. Clarendon Press, Oxford. (488 pp).

Du, Z., Allan, N.L., Blundy, J.D., Purton, J.A., Brooker, R.A., 2008. Atomistic simulation of the mechanisms of noble gas incorporation in minerals. Geochim. Cosmochim. Acta 72, 554–573.

Fechtig, H., Gentner, W., Kalbitzer, S., 1961. Argonbestimmungen an Kaliummineralien – IX. Messungen zu den verschiedenen Arten der Argondiffusion. Geochim. Cosmochim. Acta 25, 297–311.

Fick, A., 1855. Über diffusion. Ann. Phys. 94, 59–86.

Flude, S., Halton, A.M., Kelley, S.P., Sherlock, S.C., Schwanethal, J., Wilkinson, C.M., 2014. Observation of centimetre-scale argon diffusion in alkali feldspars: implications for ^{40}Ar/^{39}Ar thermochronology. Geol. Soc. London Spec. Pub. 378, 265–275.

Foland, K.A., 1994. Argon diffusion in feldspars. In: Parsons, I. (Ed.), Feldspars and their Reactions. Kluwer, Dordrecht, pp. 415–447.

Fourier, J.-B.J., 1822. Théorie analytique de la chaleur. Didot, Paris, 647 pp.
Freeman, J.J., Wang, A.L., Kuebler, K.E., Jolliff, B.L., Haskin, L.A., 2008. Characterization of natural feldspars by Raman spectroscopy for future planetary exploration. Can. Mineral. 46, 1477–1500.
Gordon, R.B., 1959. Color centers in crystals. Am. Sci. 47, 361–365.
Hetherington, C.J., Villa, I.M., 2007. Barium silicates of the Berisal complex, Switzerland: a study in geochronology and rare-gas release systematics. Geochim. Cosmochim. Acta 71, 3336–3347.
Lasaga, A.C., 1981. The atomistic basis of kinetics: defects in minerals. Rev. Mineral. 8, 261–319.
Laves, F., 1956. Über die Bedeutung der Barbierit-Analbit-Umwandlung (displacive transformation) für die Erscheinungsformen der Feldspäte in Larvikiten und Rhombenporphyren. Z. Krist. 107, 196–201.
Liu, W.D., Yang, Y., Zhu, K.Y., Xia, Q.K., 2018. Temperature dependences of hydrous species in feldspars. Phys. Chem. Miner. 45, 609–620.
McKeown, D.A., 2005. Raman spectroscopy and vibrational analysis of albite: from 25 °C through the melting temperature. Am. Mineral. 90, 1506–1517.
Nyfeler, D., Armbruster, T., Villa, I.M., 1998. Si, Al, Fe order-disorder in Fe-bearing K-feldspar from Madagascar and its implication to Ar diffusion. Schweiz. Mineral. Petrogr. Mitt. 78, 11–21.
Panzarini, G., Colombo, L., 1994a. Hydrogen diffusion in silicon from tight-binding molecular dynamics. Phys. Rev. Lett. 73, 1636–1639.
Panzarini, G., Colombo, L., 1994b. Hydrogen diffusion in crystalline silicon: a tight-binding molecular dynamics study. Phase Transit. 52, 137–149.
Richet, P., Mysen, B.O., Ingrin, J., 1998. High-temperature X ray diffraction and Raman spectroscopy of diopside and pseudowollastonite. Phys. Chem. Miner. 25, 401–414.
Salje, E.K.H., 1986. Raman-spectroscopic investigation of the order parameter behavior in hypersolvus alkali feldspar - displacive phase-transition and evidence for Na-K site ordering. Phys. Chem. Miner. 13, 340–346.
Stangarone, C., Angel, R.J., Prencipe, M., Campomenosi, N., Mihailova, B., Alvaro, M., 2019. Measurement of strains in zircon inclusions by Raman spectroscopy. Eur. J. Mineral. 31, 685–694.
Turner, G., Huneke, J.C., Podosek, F.A., Wasserburg, G.J., 1971. ^{40}Ar–^{39}Ar ages and cosmic ray exposure age of Apollo 14 samples. Earth Planet. Sci. Lett. 12, 19–35.
Villa, I.M., 1996. The influence of irradiation and heating schedule on Ar diffusion in gem-quality orthoclase from Madagascar. J. Conf. Abs. 1, 652.
Villa, I.M., 2021. The in vacuo release of Ar from minerals: 1. hydrous minerals. Chem. Geol. 564, 120076.
Wartho, J.A., Kelley, S.P., Brooker, R.A., Carroll, M.R., Villa, I.M., Lee, M.R., 1999. Direct Ar diffusion measurements in a gem-quality Madagascar K-feldspar using the Ultra-Violet Laser Ablation Microprobe (UVLAMP). Earth Planet. Sci. Lett. 170, 141–153.
Wenk, H.-R., 1978. Ordering of the intermediate plagioclase structure during heating. Am. Mineral. 63, 132–135.
Yang, H., Finger, L.W., Conrad, G., Prewitt, C.T., Hazen, R.M., 1999. A new pyroxene structure at high pressure: single-crystal X ray and Raman study of the pbcn –P21cn phase transition in protopyroxene. Am. Mineral. 84, 245–256.
Zeiger, H.J., Vidal, J., Cheng, T.K., Ippen, E.P., Dresselhaus, G., Dresselhaus, M.H., 1992. Theory for displacive excitation of coherent phonons. Phys. Rev. B 45, 768–778.
Zhang, M., Wruck, B., Barber, A.G., Salje, E.K.H., Carpenter, M.A., 1996. Phonon spectra of alkali feldspars: phase transitions and solid solutions. Am. Mineral. 81, 92–104.